







Transport signatures of magnetic texture evolution in a microfabricated thin plate of antiskyrmion-hosting (Fe, Ni, Pd)₃P

Daisuke Nakamura ^{1,*}, Kosuke Karube ¹, Keisuke Matsuura ¹, Fumitaka Kagawa ^{1,2}, Xiuzhen Yu ¹,
Yoshinori Tokura,^{1,3} and Yasujiro Taguchi ¹

¹RIKEN Center for Emergent Matter Science (CEMS), Wako 351-0198, Japan

²Department of Physics, Tokyo Institute of Technology, Tokyo 152-8551, Japan

³Tokyo College and Department of Applied Physics, University of Tokyo, Tokyo 113-8656, Japan



(Received 15 March 2023; revised 19 July 2023; accepted 3 August 2023; published 1 September 2023)

Field-induced evolution of magnetic textures in a spatially confined geometry is investigated by transport and imaging techniques for a microfabricated thin plate of antiskyrmion-hosting ferromagnet (Fe, Ni, Pd)₃P. Magnetic textures and accompanying transport characteristics show history-dependent evolution under the magnetic fields. In the up-sweep of magnetic field for a metastable antiskyrmion state, the longitudinal and Hall resistivity monotonously develop without conspicuous anomalies, due to the gradual shrinkage of the topologically-protected antiskyrmions in size. On the other hand, a row of magnetic bubbles and/or a stripe domain sequentially emerges one by one in a discretized manner upon decreasing magnetic field from the field-polarized single domain state. This gives rise to contrasting behavior with the field-increasing process, namely anomalous jumps in Hall resistivity at the several field values that are dictated by the sample and magnetic texture sizes, over a broad temperature range. Micromagnetic simulations reproduce qualitative features of the down-sweep process well, and also indicate the importance of the inherent small uniaxial magnetic anisotropy. Our work demonstrates that such a microfabricated magnetic device with a comparable size of magnetic texture may enable an electrical readout of magnetic states.

DOI: [10.1103/PhysRevB.108.104403](https://doi.org/10.1103/PhysRevB.108.104403)

I. INTRODUCTION

Ferromagnetic materials often form complex domain structures to reduce magnetostatic energy at the cost of domain-wall energy, and the shape and size of the domains and domain walls are self-organized so that the total energy including Zeeman energy may be minimized, depending on many parameters, such as exchange interaction, magnetic anisotropy, saturation magnetization, sample size and shape, magnetic field, etc. The conventional domain patterns include stripes and bubbles [1–3], the latter of which have recently attracted renewed interest due to the intensive investigations on topological magnetic textures [4–7], such as skyrmions [8–10] and antiskyrmions [11,12].

Towards application of the magnetic textures for spintronics, one crucial and fundamental issue is to understand how they emerge and annihilate in a confined mesoscopic system upon changing temperature and magnetic field and how the emergence and annihilation are reflected in transport characteristics [13]. In bulk ferromagnets with a huge number of domains, field-induced change of the domain pattern is detected transiently via the Faraday's law, widely known as the Barkhausen noise [14], but not by static probes with sufficient sensitivity. As the sample size is reduced and becomes comparable with the domain size, however, the change of magnetic texture may manifest itself in transport characteristics, especially in the anomalous Hall effect. Elucidating how magnetic

textures emerge and evolve in the reduced-size sample is an intriguing issue for mesoscopic magnetism, yet to be fully clarified.

We attempt to focus on the transport properties associated with the field-induced evolution of magnetic textures for a mesoscopic sample of a ferromagnet with weak uniaxial anisotropy, which may enhance the controllability of magnetic texture. We investigate the transport properties, whereas, comparing with the magnetic textures obtained by magnetic force microscopy (MFM) imaging for a thin plate of an antiskyrmion-hosting (Fe, Ni, Pd)₃P. The antiskyrmion, which is composed of four Bloch-type domain walls and four Néel-type walls at the intersections [Fig. 1(a)] [11,12,15–23], is stabilized by the dipolar interaction [24] and anisotropic Dzyaloshinskii-Moriya (DM) interaction [25,26] and was first observed in Mn_{1.4}Pt_{0.9}Pd_{0.1}Sn with D_{2d} symmetry [11]. More recently, (Fe_{0.63}Ni_{0.30}Pd_{0.07})₃P with S_4 symmetry was also found to host antiskyrmions [17]. In this paper, history-dependent transport characteristics are found, depending on the different magnetic textures. In a field-increasing process for a metastable antiskyrmion state, longitudinal (ρ_{xx}) and Hall (ρ_{yx}) resistivity both evolve gradually without any conspicuous jumps, whereas, in the field-decreasing process from a fully polarized single-domain state, several discontinuous jumps are observed in ρ_{xx} and ρ_{yx} . Such anomalous jumps are ascribed to sequential emergence of a row of magnetic bubbles and/or a stripe domain [Fig. 1(b)] with discretized field intervals that are dictated by the relationship between the size of emergent magnetic texture and sample width, namely, the number of horizontal stripe domains present at zero field.

*daisuke.nakamura.rg@riken.jp

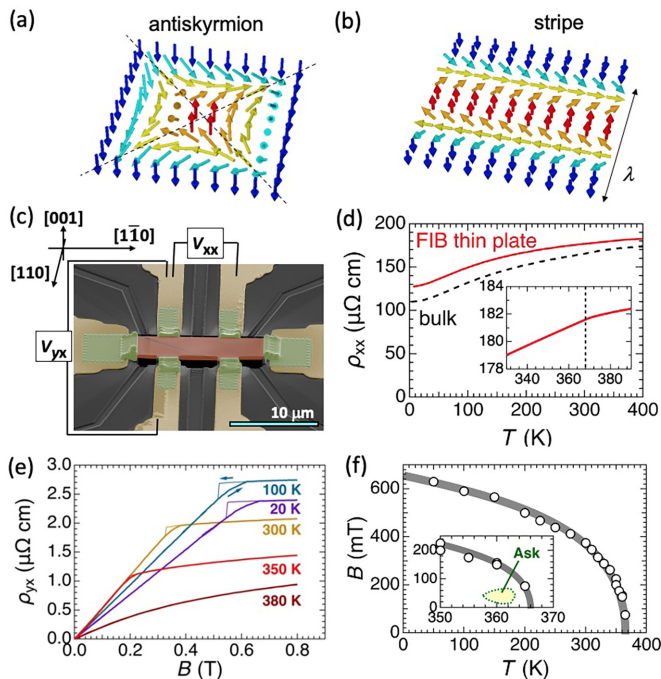


FIG. 1. Schematic of (a) antiskyrmion and (b) stripe domain texture. Dashed lines in (a) show Néel wall parts of the antiskyrmion, and λ in (b) indicates the period of the stripe domains. (c) A scanning electron microscope image of an $(\text{Fe, Ni, Pd})_3\text{P}$ thin plate fabricated by the FIB milling; pink: $(\text{Fe, Ni, Pd})_3\text{P}$, yellow: gold (Au) electrode, and green: tungsten (W) pad. The colored scale bar represents $10\ \mu\text{m}$. (d) Temperature dependence of the electrical resistivity of the FIB-fabricated thin plate (solid curve) and of a bulk sample (dashed curve). The inset is an enlarged view close to T_c (indicated by the vertical line). (e) Magnetic-field dependence of Hall resistivity at selected temperatures. The thick (thin) curves are the data for up-sweep (down-sweep) processes of the magnetic field. (f) Magnetic phase diagram determined from the Hall resistivity data. The open symbols are the transition fields into a forced single-domain ferromagnetic state. The inset is an enlarged view near T_c where the equilibrium Ask expected from Lorentz TEM experiment [18] is shown.

II. EXPERIMENT

$(\text{Fe}_{0.60}\text{Ni}_{0.32}\text{Pd}_{0.08})_3\text{P}$ single crystals were prepared by a self-flux method as described in Ref. [27]. The chemical composition of bulk crystal and the thin plate used in this paper was almost the same within the experimental error, which was evaluated by using an energy dispersive x-ray spectroscopy. From a bulk crystal piece, we fabricated a thin plate sample with a Hall bar structure with $5 \times 15 \times 0.75\ \mu\text{m}^3$ [Fig. 1(c)] by using a focused ion beam (FIB) instrument (NB-5000, Hitachi). The surface of the thin plate is perpendicular to $[001]$, and two sides are perpendicular to $[110]$ and $[1\bar{1}0]$. Gold electrodes with 150-nm thickness were patterned on a Si substrate by using a maskless ultraviolet photolithography system (D-light-DL1000RS, Nano Sys. Solns.) and an electron-beam heating evaporation system (EB-evap, Katagiri Eng.). The thin plate sample was connected to the gold electrode pattern by the evaporation of tungsten in the FIB instrument.

Resistivity measurements were conducted by using a Physical Property Measurement System (Quantum Design), and

the typical current density of $3 \times 10^8\ \text{A/m}^2$ was applied along the $[1\bar{1}0]$ direction. Because of the stochastic feature of magnetic texture evolution in a microfabricated sample, we do not perform symmetrization and antisymmetrization with respect to $\pm B$ for ρ_{xx} and ρ_{yx} , respectively. For ρ_{yx} , only $\rho_{yx}(B=0)$ is subtracted from the raw data.

Imaging of the magnetic texture at ambient temperature was performed by using the atomic force microscope (MFP-3D, Asylum Research) and an MFM cantilever (MFMR, Nano World). The lift height of an MFM cantilever was typically 50 nm above the sample surface. For the MFM measurement under magnetic fields, a Nd-based permanent magnet was attached under a Si substrate with the $(\text{Fe, Ni, Pd})_3\text{P}$ thin plate (details are described in the Supplemental Material, Section C-1 [28]).

III. RESULTS AND DISCUSSIONS

The temperature dependence of the electrical resistivity of the $(\text{Fe, Ni, Pd})_3\text{P}$ thin plate is almost the same as that of a bulk sample as shown in Fig. 1(d), indicating that the fabrication process using an FIB technique does not change the sample characteristics. The magnetic transition temperature T_c is evaluated to be 367 K from an anomaly of resistivity [the inset of Fig. 1(d)]. Figure 1(e) shows the magnetic-field dependence of Hall resistivity ρ_{yx} at different temperatures. The $\rho_{yx}(B)$ is dominated by the anomalous Hall effect, i.e., the relation that $\rho_{yx} \propto M$ almost holds. For the $(\text{Fe, Ni, Pd})_3\text{P}$ thin plate with the thickness of $1\ \mu\text{m}$, the period of the magnetic texture is determined to be $\lambda \sim 700\ \text{nm}$ [17]. When the quantum flux (h/e) of antiskyrmion forms a lattice with the interval of λ , the emergent magnetic field can be evaluated as 8.4 mT. Therefore, the contribution of topological Hall effect [4] is hardly discernible in the present sample due to a small value of emergent magnetic field, whereas, reported in other antiskyrmion-hosting materials [29–34]. Below T_c , there is a clear hysteresis loop in $\rho_{yx}(B)$ near the magnetic saturation field, whose magnitude increases with decreasing temperature. A steep jump in ρ_{yx} at the transition from the field-polarized single-domain state indicates that a magnetic texture suddenly appears in a discontinuous manner in the down-sweep process, similar to previous observations in thin films or thin plates [32,35–39].

From ρ_{yx} data in the up-sweep process of the magnetic field, the saturation field is determined as presented in Fig. 1(f). In the enlarged view (the inset), the thermodynamic equilibrium antiskyrmion phase (Ask) expected from the Lorentz transmission electron microscopy (TEM) experiment [18] is depicted with a dotted encircling curve (see Supplemental Material, Section A for details [28]). Only when the temperature is decreased across the Ask phase under $B_0 \sim 40\ \text{mT}$ [B_0 : the magnetic-field value of the field-cooling (FC) process], the metastable antiskyrmions are anticipated to persist in a wide range of the magnetic-phase diagram [18].

A. Magnetic textures that depend on the field-cooling process

We confirm that the magnetic texture in the $(\text{Fe, Ni, Pd})_3\text{P}$ thin plate used in this paper changes, depending on FC conditions [paths 1–4, Fig. 2(a)]. Figures 2(b)–2(e) are MFM phase images captured at zero field and at ambient

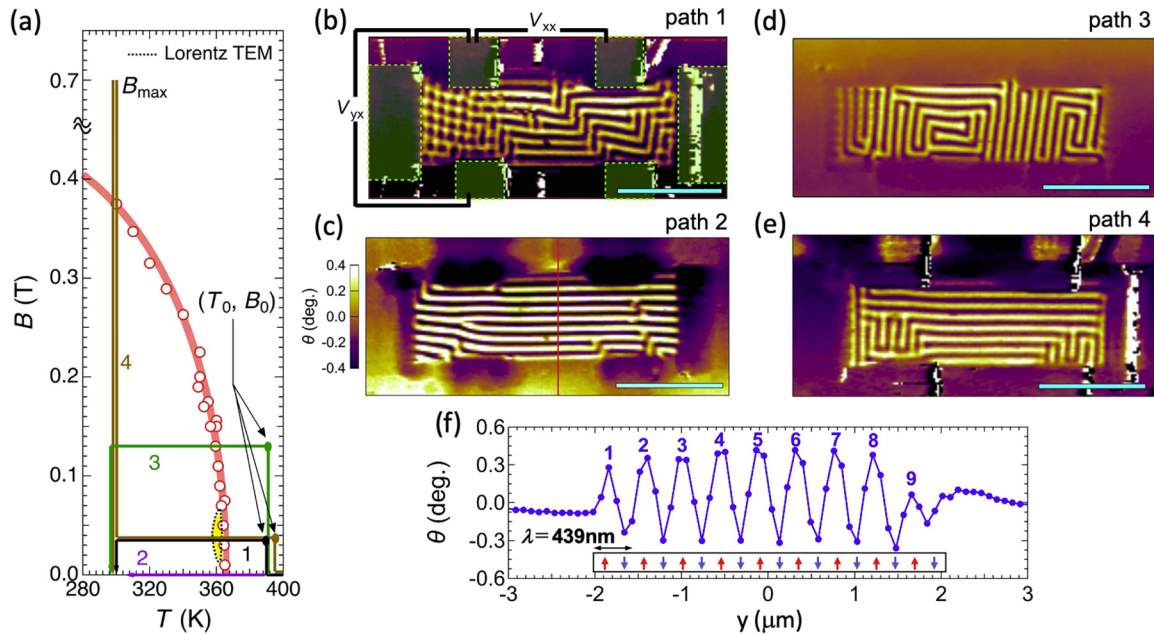


FIG. 2. (a) Paths 1–4 of the FC process performed before the MFM measurements are shown. The yellow-shaded region encircled by a dotted line indicates the equilibrium antiskyrmion phase expected from the Lorentz TEM experiments [18]. The open symbols indicate the transition fields into a forced single-domain ferromagnetic state. (T_0, B_0) is the starting point of a FC process; $(T_0, B_0) = (385 \text{ K}, 0 \text{ mT})$ for path 1, $(390 \text{ K}, 0 \text{ mT})$ for path 2 (zero-field cooling), $(385 \text{ K}, 130 \text{ mT})$ for path 3, and $(390 \text{ K}, 35 \text{ mT})$ for path 4. For path 4, after the FC to 300 K, a magnetic field of B_{max} (well above the saturation field) is once applied and removed, and then, an MFM image is captured at zero magnetic field. (b)–(e) Magnetic texture images observed by the MFM measurements at zero field and at ambient temperature after the FC processes 1–4 shown in (a). The blue scale bars represent $5 \mu\text{m}$. (f) The phase of an MFM signal (θ) along the vertical axis (y axis) of the sample plate indicated by a red line in (c). Electrodes for the transport measurements are indicated in panel (b) with light-green rectangles.

temperature after following the paths 1–4, respectively. The image taken through the path 1 [Fig. 2(b)] exhibits a magnetic texture qualitatively different from others. A squarelike lattice structure is clearly seen at the left-hand side of the thin plate. This suggests that the antiskyrmions with dipolar interaction [24] are created by the FC process and subsist outside the thermodynamic equilibrium phase. The number of observed antiskyrmions in the thin plate becomes largest with the cooling field $B_0 \sim 35 \text{ mT}$, being consistent with the result of the Lorentz TEM experiment (see Supplemental Material, Section A [28] and [18]). The emergence of antiskyrmions only in a limited area of the sample [Fig. 2(b)] implies the effect of some stress possibly acting on the thin plate and may also arise from a rather slow cooling speed of $\sim 0.1 \text{ K/s}$ for a larger rectangular sample as compared with the previous work [18].

For the paths 2 and 3, there are no antiskyrmion texture discernible in the plate. A horizontal stripe texture is observed for zero-field-cooling (ZFC) case [path 2, Fig. 2(c)], whereas the direction of some stripes changes to vertical for the FC case with $B_0 = 130 \text{ mT}$ [path 3, Fig. 2(d)]. The competition between the domain-wall energy and the demagnetization energy in a mesoscopic system could change the most stable orientation of stripe texture under the magnetic field. The anisotropy in the exchange coupling and DM interaction might also slightly change in the FC process via the magnetostriction effect. A period of stripe texture in Fig. 2(c) is evaluated to be $439 \pm 1 \text{ nm}$ on average as shown in Fig. 2(f). There are nine peaks and dip structures, which correspond to the nine domains of up- and down-magnetization, respectively.

For path 4 [Fig. 2(e)], there is no antiskyrmion, whereas, the horizontal stripe texture is dominant. This indicates that the antiskyrmions once created by the FC process are completely annihilated by a high magnetic field above the saturation and do not recover at zero magnetic field after the field down-sweep at 300 K.

B. Transport anomalies with sequential emergence of stripe domain

Reflecting the difference in emergent magnetic textures depending on the magnetic field and FC histories, $\rho_{yx}(B)$ in the field-increasing process after the creation of metastable antiskyrmions can exhibit different behavior from that in the field-decreasing process from the field-polarized single-domain ferromagnetic state. Figures 3(a) and 3(b) show the magnetic-field dependence of longitudinal resistivity ρ_{xx} (top panel) and Hall resistivity $\rho'_{yx}(= \rho_{yx} - \alpha B)$ (bottom panel) at 300 K measured after the FC and ZFC processes, respectively. Here, the B -linear term is subtracted for the purpose of clarity in Hall resistivity. For the FC process to create metastable antiskyrmions, $B_0 = 35 \text{ mT}$ is applied. In Fig. 3(a), a hysteresis between up-sweep (bold curves) and down-sweep (thin curves) of the magnetic field appears both in ρ_{xx} and ρ'_{yx} , and the hysteresis is substantially enhanced as compared with the result of ZFC process shown in Fig. 3(b).

In the up-sweep process after the FC, ρ_{xx} and ρ'_{yx} gradually evolve with the magnetic field without any discontinuous changes. By contrast, in the down-sweep process, an abrupt

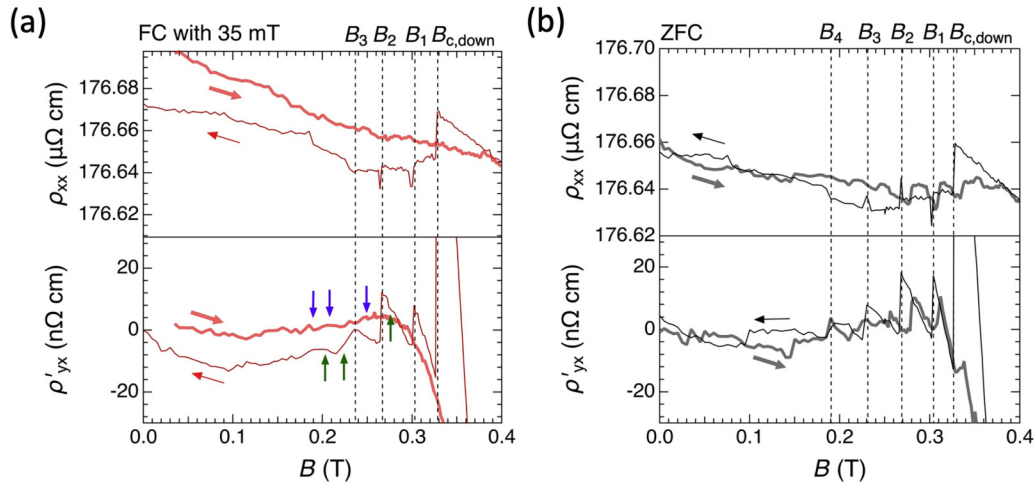


FIG. 3. Magnetic-field dependence of the electrical resistivity at 300 K after (a) a FC process with 35 mT and (b) a ZFC process. The measurements are performed for exactly the same thin plate sample as probed by MFM. In the top and bottom panels, longitudinal resistivity ρ_{xx} and Hall resistivity ρ_{yx} are plotted, respectively, in which B -linear contribution in ρ_{yx} is subtracted for a clearer view; $\rho'_{yx} = \rho_{yx} - \alpha B$. The bold and thin curves are the data of up- and down-sweep processes of the magnetic field, respectively. The magnetic-field values exhibiting anomalous jumps in ρ'_{yx} are denoted as $B_{c,down}$ and B_i ($i = 1-4$). In (a), the blue and green arrows indicate the magnetic field values where the MFM images in Figs. 5(b)–5(d) and 5(f)–5(h) are acquired, respectively.

jump in ρ'_{yx} appears at the critical field ($B_{c,down}$), as already noted in Fig. 1(e). Then, with decreasing the magnetic field furthermore, we find several smaller but clear jumps in ρ'_{yx} at B_i ($i = 1-4$), accompanied by peak or dip anomalies in ρ_{xx} . This qualitative difference between up-sweep and down-sweep processes strongly indicates the existence of different magnetic textures in both processes. The discernible jumps in ρ'_{yx} at $B_{c,down}$ and B_i ($i = 1-3 \dots$) only appear in the thin plate and not in a bulk sample. This suggests that the characteristic size of magnetic texture comparable with the sample size is relevant to the emergence of the anomalous jumps in ρ'_{yx} .

The magnetic textures at zero field after the similar FC and after decreasing the field from the field-polarized single-domain state are shown in Figs. 2(b) and 2(e), and the Hall resistivity is monitored with the left-hand side Hall probes as indicated in Fig. 2(b). The metastable antiskyrmions are formed on the left side of thin plate after the FC process [Fig. 2(b)] and the horizontally running stripe texture is observed after decreasing the field from the field-polarized single-domain state [Fig. 2(e)]. Therefore, in the up-sweep process, the carriers are expected to flow through the metastable antiskyrmions created by the FC process. Due to the topologically protected nature, the size of antiskyrmions could gradually shrink (at least, up to some field value) upon increasing the magnetic field, resulting in the absence of discontinuous changes in ρ_{xx} and ρ'_{yx} . Such a gradual shrinkage of antiskyrmions has been observed in different (Fe, Ni, Pd)₃P thin plates by the previous Lorentz TEM experiments [18] (also see the Supplemental Material, Fig. S6 [28]). By contrast, in the down-sweep process, the successive jumps observed mainly in ρ'_{yx} suggest a discontinuous change in the magnetic texture since ρ_{yx} is dominated by the anomalous term that represents the total magnetization of the measured channel of the sample.

The transport data after the ZFC process shown in Fig. 3(b) are also consistent with the working hypothesis of the evo-

lution of magnetic texture. Several jumps are found in ρ'_{yx} both in the up-sweep and down-sweep measurements. The magnetic texture after the ZFC process is confirmed to be the stripe domains as shown in Fig. 2(c), similar to that after the down-sweep process shown in Fig. 2(e). Therefore, the observed jumps in ρ'_{yx} are likely to originate from the discontinuous changes in the stripe texture pattern.

In Fig. 3, the jump in ρ'_{yx} always reduces its value upon decreasing the field, whereas, the polarity of the anomalies (peak or dip) in ρ_{xx} does not show apparent regularity. The negative change of ρ'_{yx} reflects a decrease in total magnetization when the magnetic texture changes. On the other hand, the sign of the jump in ρ_{xx} depends on the specific change in the detailed topology and configuration of the magnetic domains at B_i as it perhaps arises from the scattering by the domain wall. This may be the reason for the nonregular feature in the sign of the jump in ρ_{xx} .

To gain insights into the relationship between the transport and the magnetic texture in the down-sweep process, the sequential jumps in ρ'_{yx} at the fields $B_{c,down}$ and B_i ($i = 1-3 \dots$) are analyzed in detail. The magnitude of the jump in ρ'_{yx} at $B_{c,down}$, $\Delta\rho_{yx}$, is normalized by $\rho_{yx}(B_{c,down})$ and plotted against temperature in Fig. 4(a) (The raw data of $\rho_{xx}(B)$ and $\rho_{yx}(B)$ at selected temperatures are shown in the Supplemental Material, Fig. S2 [28]). The value of $\Delta\rho_{yx}/\rho_{yx}(B_{c,down})$ monotonically increases with decreasing temperature, and approaches 1/9 towards absolute zero temperature. The differences between B_i ($i = 1-3 \dots$) and $B_{c,down}$, $\Delta B_i = B_{c,down} - B_i$'s, are also normalized and plotted in Fig. 4(b). $\Delta B_i/B_{c,down}$ for $i = 1-4$ gradually decreases upon decreasing temperature with the same temperature coefficient. Most of the data well collapse on the solid lines in Fig. 4(b) which pass through $i \times (1/9)$ at T_c and $(i-1) \times (1/8)$ at 0 K, suggesting a regular feature of the changes in the magnetic texture pattern. Exceptionally, only $\Delta B_1/B_{c,down}$ increases again below 100 K as shown by the bold dashed

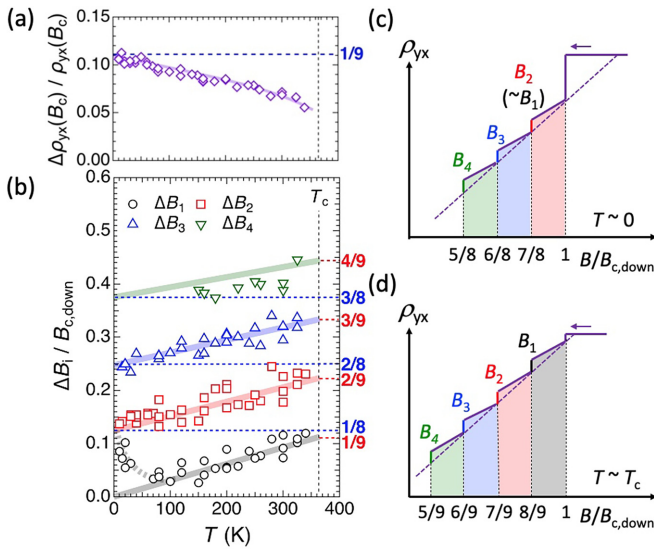


FIG. 4. (a) Temperature dependence of the magnitude of the jump in Hall resistivity at $B_{c,down}$, $\Delta\rho_{yx}$, normalized by the Hall resistivity value in the single-domain ferromagnetic state. (b) Temperature variation of the magnetic-field intervals between B_i and $B_{c,down}$, $\Delta B_i = B_{c,down} - B_i$. For the bold lines, see the text. With decreasing temperature, the field B_1 gradually approaches $B_{c,down}$, and then turns to separate from $B_{c,down}$ below 100 K. Finally, close to $T = 0$, B_1 almost merges to B_2 . (c) and (d) Schematics of $\rho_{yx}(B)$ at $T \sim 0$ and $T \sim T_c$. The difference of magnetic textures is represented as different colors.

line, possibly because nucleation of magnetic textures tends to be more difficult at low temperatures (The MFM images at low temperature are shown in the Supplemental Material, Fig. S5 [28]).

On the basis of the results in Figs. 4(a) and 4(b), ρ_{yx} with the anomalous jumps in the down-sweep process is schematically drawn in Fig. 4(c) for $T \sim 0$ K and Fig. 4(d) for $T \sim T_c$, respectively. At $T \sim 0$, a large jump of $(1/9) \times \rho_{yx}(B_{c,down})$ takes place at $B_{c,down}$, and then smaller jumps occur with an interval of $(1/8) \times B_{c,down}$, corresponding to nine steps in total (although steps beyond B_4 are not clearly discerned). At $T \sim T_c$, the hysteresis at $B_{c,down}$ becomes significantly small, and the tiny jumps in ρ_{yx} take place with an interval of $(1/9) \times B_{c,down}$, suggesting that the interval also corresponds to nine steps, independent of the temperature. As seen in the analysis of the MFM image [Fig. 2(f)], the $(\text{Fe, Ni, Pd})_3\text{P}$ thin plate used in this work exhibits nine horizontal stripes at zero magnetic field after the ZFC process. Therefore, it can be conjectured that the number of horizontally running stripe domains changes sequentially at each B_i , rather than continuous expansion of the width of opposite-magnetization domains.

Despite a rather simple evolution process of magnetic texture pattern naturally expected for the confined geometry, to the best of our knowledge, there has been no experimental report of the discretized multiple step structures in anomalous Hall resistivity (while discretized topological Hall resistivity is observed upon changing the number of skyrmions in nanostructured Hall bar devices [13]). As long as the discontinuous jump in ρ_{yx} at $B_{c,down}$ is concerned, there are similar cases in thin-plate samples of uniaxial ferromagnets [32,38,39]. How-

ever, the magnetic texture just below $B_{c,down}$ totally depends on each material: In $\text{Mn}_{1.4}\text{PtSn}$ [32,38], many straight stripe domains suddenly appear all over the sample, whereas, a maze pattern appears throughout the sample in $\text{Nd}_2\text{Fe}_{14}\text{B}$ [39]. These results are different from the working hypothesis for the present $(\text{Fe, Ni, Pd})_3\text{P}$ thin-plate sample where the number of horizontal rows of opposite magnetization domains increases one by one below $B_{c,down}$. Such a sequential emergence of the magnetic texture can be identified as schematically shown by different colors in Figs. 4(c) and 4(d).

C. Evolution of magnetic texture under the magnetic field

For a direct observation of the evolution in magnetic textures, MFM images are captured for the $(\text{Fe, Ni, Pd})_3\text{P}$ thin plate on a permanent magnet with use of a field up-sweep and down-sweep protocols shown in Figs. 5(a) and 5(e). To change the measurement field B_m , we use several permanent magnets with different field intensities (see the Supplemental Material, Section C-1 for details [28]). Figures 5(b)–5(d) show the MFM images with different B_m s in the up-sweep process of the magnetic field. At $B_m = 190$ mT [Fig. 5(b)], the antiskyrmion and stripe textures, respectively, emerge on the left- and right-hand sides of the thin plate, similar to the case of Fig. 2(b). With increasing B_m , the antiskyrmions remain intact, whereas, the stripe texture is gradually replaced with the dotlike antiskyrmion texture [Figs. 5(c) and 5(d)]. The replacement from the stripe texture to antiskyrmion by applying the magnetic field has also been observed in the Heusler compound [21,39,40] and predicted by calculations [41].

In the down-sweep protocols, dotlike magnetic textures are observed in MFM image at $B_m = 276$ mT [Fig. 5(f)], whereas, stripe domains are dominant over the whole surface of the thin plate below $B_m = 224$ mT [Figs. 5(g) and 5(h)]. Importantly, the number of the horizontally running magnetic textures (bubbles or stripes) sequentially increases upon decreasing the field. This is the experimental evidence supporting our working hypothesis deduced from the sequential jumps in ρ_{yx} . The values of B_m shown in Fig. 5 are indicated by the blue and green arrows in Fig. 3(a) for up-sweep and down-sweep conditions, respectively. In the down sweep, B_m of 276 mT locates between B_1 and B_2 exhibiting jumps in ρ_{yx} . When the first horizontally running line of magnetic texture appears at $B_{c,down}$, and then the second one appears at B_1 , the two lines of the horizontally running texture are expected to exist at 276 mT, which is indeed confirmed in Fig. 5(f). For B_m of 224 and 203 mT just below B_3 as indicated in Fig. 3(a), the four lines of horizontally running texture are expected by a similar argument. As expected, the fourth horizontally running stripe domain develops from the bottom right of the thin plate in Figs. 5(g) and 5(h). We confirm the sequential evolution of the horizontally running stripe domains and magnetic bubbles also in the up-sweep run after the ZFC process corresponding with the bold curves in Fig. 3(b) as shown in the Supplemental Materials, Fig. S4 [28].

The characteristic sequential emergence of magnetic textures indicates that simultaneous nucleation of many horizontal rows of domains is difficult to happen in the microfabricated thin plate, probably due to the comparable size between the thin plate and the magnetic textures as

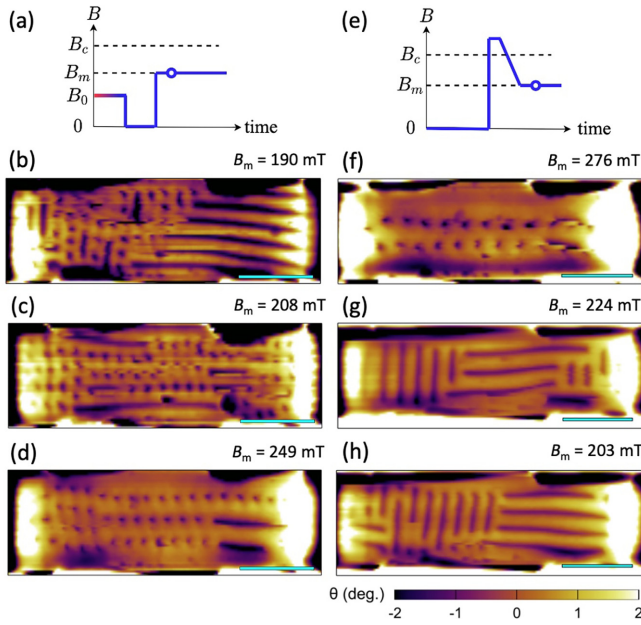


FIG. 5. (a) MFM experiment protocol for the up-sweep of the magnetic field. The initial line with color gradation (from red to blue) represents the FC process from above T_c to ambient temperature. B_0 is the magnitude of the magnetic field of the FC process by way of the thermodynamic antiskyrmion phase region, B_m is magnitude of the magnetic field for the MFM measurements as indicated by the open circle, B_c is the magnetic saturation field. The $(\text{Fe, Ni, Pd})_3\text{P}$ thin plate was mounted on a permanent magnet after a FC process with $B_0 = 35$ mT. After each MFM measurement at (b) 190, (c) 208, and (d) 249 mT, the FC process was repeated, and the thin plate was mounted on a different permanent magnet. In this protocol, the antiskyrmion texture is observed as shown in Fig. 2(b), before mounting on a permanent magnet. (e) Experimental protocol for MFM measurements in the down-sweep process of the magnetic field. A magnetic field above B_c was applied at ambient temperature and then gradually decreased to B_m with a typical speed of 0.02 T/min. (f)–(h) The MFM images with different B_m 's; (f) 276, (g) 224, and (h) 203 mT. The blue scale bars represent 3 μm . The contrast in the MFM images largely changes near the edge of the thin plate due to a steep field gradient, which makes the magnetic texture obscure to visualize. Therefore, we made calibrations along the vertical direction for the MFM images (see the Supplemental Material, Section C-1 for details [28]).

observed in Heusler compound [21] as well as to the position-dependent demagnetizing field in the small sample plate [42]. Indeed, when the period of magnetic texture is decreased by reducing the sample thickness, with keeping the lateral dimensions of a thin plate, a series of discontinuous jumps in ρ_{yx} are still observed but become somewhat ambiguous due to the reduced degree of the size matching (see the Supplemental Material, Section F [28]).

D. Micromagnetic simulations

To obtain better understanding for the evolution of magnetic textures in the down-sweep process observed in Fig. 5, we perform the micromagnetic simulation by using MuMax³

[43]. We use the following energy functional:

$$E(\vec{m}) = \int_V \left\{ A(\nabla\vec{m})^2 + D[\vec{m} \cdot (\vec{e}_x \times \partial_x\vec{m}) - \vec{m} \cdot (\vec{e}_y \times \partial_y\vec{m})] - K_u(\vec{m} \cdot \vec{e}_z)^2 - \frac{M_s}{2}\vec{m} \cdot \vec{B}_d - M_s\vec{m} \cdot \vec{B}_{\text{ext}} \right\} dV,$$

where A is the exchange stiffness, \vec{m} is the normalized magnetization, D is the DM interaction constant, K_u is uniaxial anisotropy, $\vec{e}_{x,y,z}$ is the unit vector along the x , y , and z directions, M_s is the saturation magnetization, \vec{B}_d is the demagnetizing field, \vec{B}_{ext} is the external field, and V is the volume of the thin plate. We take into account the anisotropic DM interaction ($D_x = -D_y$), similar to Ref. [17]. The simulated sample size is $2.25 \times 0.75 \times 0.075 \mu\text{m}^3$ with the open boundary condition, which is approximately one order of magnitude smaller in size than that used in experiments, whereas, keeping the aspect ratio between the width and the length to reduce the simulation time. The simulated sample volume was discretized to $512 \times 128 \times 16$ cells. The parameters used in the simulation are based on those experimentally evaluated in the previous reports [17,27]; $A = 8.1$ pJ/m, $D = 0.2$ mJ/m², $M_s = 540$ kA/m, and $K_u = 62$ kJ/m³. We note that K_u is exceptionally set to be two times larger than the previous report [17] to compensate the change in the demagnetization field. The smaller ratio of thickness to the lateral dimensions gives rise to an enhanced demagnetization field as compared with that deduced from the experiments [27]. All magnetizations are oriented along the z direction under the applied field of 1.0 T, and the field magnitude is gradually decreased. Then, the system is relaxed at each field value to find a magnetization arrangement with a local energy minimum.

The simulated magnetization curve and corresponding magnetic textures with different external fields in the down-sweep process are displayed in Figs. 6(a) and 6(b)–6(g), respectively. With decreasing the magnetic field from the single-domain ferromagnetic state, small in-plane magnetization first appears [Fig. 6(b)], next several magnetic bubbles forming a horizontal row emerge [Fig. 6(c)], and then the second horizontal row appears with decreasing the magnetic field [Fig. 6(d)]. Upon further decreasing the field, the magnetic bubbles transform into the stripe texture [Fig. 6(e)], and the number of the horizontally running stripes increases again [Figs. 6(f) and 6(g)]. Such an evolution of magnetic texture during the field-decreasing process is qualitatively the same as observed in the MFM images shown in Figs. 5(f)–5(h), although full agreement in a quantitative level is not attained due to the difference in the system size (and demagnetization effect) between the experiment and the simulation.

We find that small uniaxial anisotropy in $(\text{Fe, Ni, Pd})_3\text{P}$ could promote the sequential emergence of the magnetic textures. Emergent magnetic textures just below B_c depending on the value of the uniaxial anisotropy constant K_u are simulated in Fig. 7, where $K_u =$ (a) 31, (b) 68, and (c) 93 kJ/m³, respectively. When K_u is small, the demagnetization effect becomes dominant and the in-plane magnetization domain is created to reduce the dipolar energy upon decreasing the magnetic field in Fig. 7(a). We note that just below B_c , a small horizontal component of magnetization δM_x emerges at the center position of the thin plate at $B = 0.55$ T due to

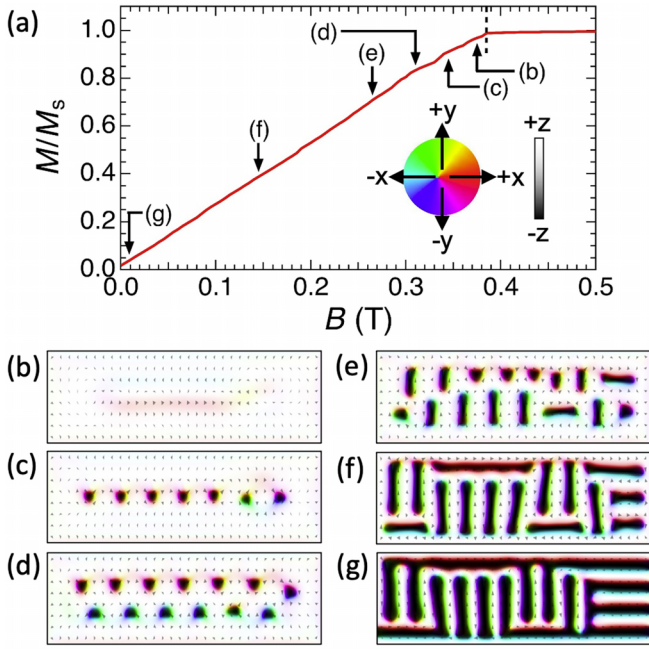


FIG. 6. (a) Simulated magnetization curve of a field down-sweep process, and (b)–(g) the averaged magnetization along the thickness direction at the selected magnetic fields below B_c [dashed line in (a)], pointed with the black arrows (b)–(g) in panel (a). The color wheel and gray-scale bar [the inset to (a)] represent the orientation of magnetization in (b)–(g).

position-dependent demagnetization effect [42]. This δM_x remains even if K_u is increased from 31 to 68 kJ/m³ as shown in Fig. 7(b). In this case, due to a slightly large K_u , the in-plane domains become energetically unstable and dotlike domains with perpendicular magnetizations start to emerge at $B = 0.42$ T. The presence of δM_x at the center of thin plate

induces a horizontal straight line of magnetic bubbles, which is similar to the experiment [Fig. 5(f)]. Fig. 7(d) represents the magnetization orientation of a single magnetic bubble at $B = 0.42$ T in the red square region of Fig. 7(b). This is a nontopological bubble with the in-plane component of magnetization aligned to the horizontal direction, which is reasonable to evolve from a small in-plane magnetization polarization δM_x at $B = 0.43$ T. When K_u is increased furthermore to 93 kJ/m³ shown in Fig. 7(c), δM_x is substantially suppressed. Therefore, nontopological bubbles with horizontal in-plane component of magnetization are not favorable, and the stripe domains emerge.

The magnetic bubble itself is a fundamental magnetic texture under moderately high magnetic fields [36], for ferromagnets with an uniaxial anisotropy. However, for a micrometer-scale thin plate, the position-dependent demagnetization effect has a strong influence on the type of emergent magnetic texture. As is seen in the diagram of simulated emergent magnetic textures as a function of K_u [Fig. 7(e)], the horizontally aligned magnetic bubbles appear in the limited region of $K_u = 45$ –85 kJ/m³. In (Fe, Ni, Pd)₃P, magnetic bubbles are induced by the demagnetization effect in such a relatively small K_u ferromagnet. In fact, K_u of (Fe, Ni, Pd)₃P is 27.9 kJ/m³ at room temperature [27], which is significantly smaller than those of other uniaxial ferromagnets exhibiting a discontinuous jump in ρ_{yx} only at $B_{c,down}$ (Mn_{1.4}PtSn: 171 kJ/m³ [38], Nd₂Fe₁₄B: 5000 kJ/m³ [44]).

IV. CONCLUDING REMARKS

As a summary of the transport and MFM measurements, and micromagnetic simulations, we schematically describe the evolution of the magnetic textures in the microfabricated thin plate of (Fe, Ni, Pd)₃P in Fig. 8. At first, the metastable antiskyrmions prepared by the FC process (U1) gradually

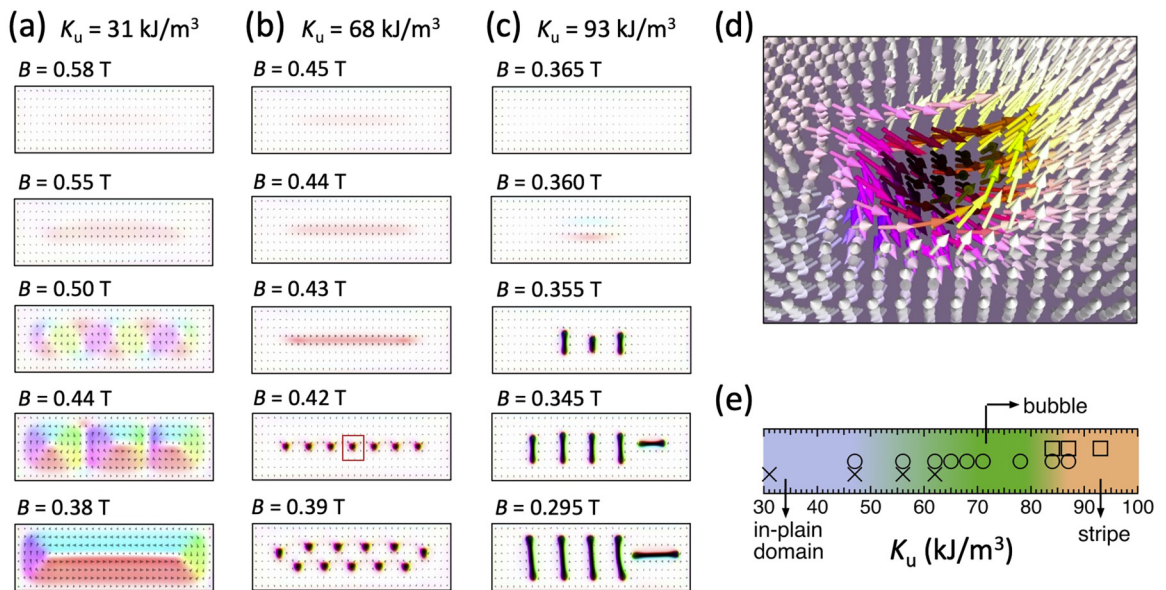


FIG. 7. Simulation results of the uniaxial anisotropy dependence. (a)–(c) Magnetic textures with different values of the magnetic field at $K_u =$ (a) 31, (b) 68, and (c) 93 kJ/m³. (d) Magnetization orientation of a single magnetic texture at $B = 0.42$ T in the red square region of (b). (e) Variation in the emergent magnetic texture just below B_c as a function of K_u .

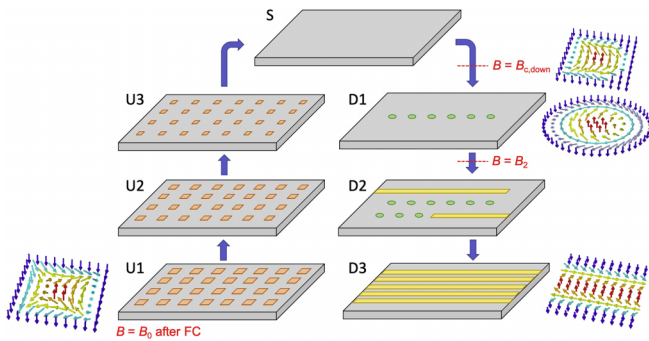


FIG. 8. Schematic of the magnetic texture patterns in the $(\text{Fe, Ni, Pd})_3\text{P}$ thin plate upon changing the magnetic field after a FC process. U1–U3 are metastable antiskyrmion textures in the up-sweep process of the magnetic field. S is the forced single-domain ferromagnetic state, D1–D3 are the magnetic textures in the down-sweep process of the magnetic field. Square, circular, and rectangular symbols indicate the antiskyrmion, nontopological bubble (or skyrmion) and stripe textures, respectively. The local magnetization patterns of corresponding textures are also illustrated.

shrink in size with increasing the magnetic field (U2 and U3). After the single-domain ferromagnetic state is attained by applying the sufficiently high magnetic field above B_c (S) and then the magnetic field is decreased, a single horizontal row of (anti)skyrmions or nontopological bubbles suddenly appears at $B_{c,\text{down}}$ (D1). Upon decreasing the magnetic field furthermore, the number of horizontal rows sequentially increases one by one, and the magnetic bubbles transform to

the stripe texture (D2 and D3) as also demonstrated in the Lorentz TEM measurement (see the Supplemental Material, Fig. S7 [28]).

The gradual shrinkage of the topologically protected metastable antiskyrmions in the field-increasing process gives rise to rather gradual variation of transport properties (both ρ_{xx} and ρ_{yx}) without discontinuous changes. By contrast, the sequential emergence of horizontal row of the magnetic bubbles or stripes in the field-decreasing process causes the anomalous jumps in Hall resistivity at several magnetic fields with discretized intervals that are governed by the relationship between the sample width and the emergent stripe width, namely, the number of horizontal stripe domains present at zero field.

These characteristic features originate from the effect of comparable size between the magnetic textures and the microfabricated thin plate in conjunction with the small uniaxial anisotropy of this material. An important point is that such an evolution of magnetic texture is identified by the electrical probe, which can serve as a useful tool in spintronic applications.

ACKNOWLEDGMENTS

We thank L. Peng, N. Nagaosa, F. S. Yasin, A. C. Collins, and M. Mochizuki for fruitful discussions. D.N. thanks K. Nakajima, RIKEN CEMS Emergent Matter Science Research Support Team and RIKEN Advanced Manufacturing Support Team for technical assistance. This work was financially supported by JST CREST (Grants No. JPMJCR20T1 and No. JPMJCR1874) and JSPS Grant-in-Aids for Scientific Research (Grants No. 20K15164 and No. 23H01841).

- [1] E. A. Giess, Magnetic bubble materials, *Science* **208**, 938 (1980).
- [2] A. Hubert and R. Schäfer, *Magnetic Domains* (Springer, Berlin, Heidelberg, 1998).
- [3] T. H. O’Dell, *Magnetic Bubbles* (Wiley, New York, 1974).
- [4] N. Nagaosa and Y. Tokura, Topological properties and dynamics of magnetic skyrmions, *Nat. Nanotechnol.* **8**, 899 (2013).
- [5] Y. Tokura and N. Kanazawa, Magnetic skyrmion materials, *Chem. Rev.* **121**, 2857 (2021).
- [6] A. Fert, N. Reyren, and V. Cros, Magnetic skyrmions: Advances in physics and potential applications, *Nat. Rev. Mater.* **2**, 17031 (2017).
- [7] K. Everschor-Sitte, J. Masell, R. M. Reeve, and M. Kläui, Perspective: Magnetic skyrmions—overview of recent progress in an active research field, *J. Appl. Phys.* **124**, 240901 (2018).
- [8] S. Mühlbauer, B. Binz, F. Jonietz, C. Pfleiderer, A. Rosch, A. Neubauer, R. Georgii, and P. Böni, Skyrmion lattice in a chiral magnet, *Science* **323**, 915 (2009).
- [9] X. Z. Yu, Y. Onose, N. Kanazawa, J. H. Park, J. H. Han, Y. Matsui, N. Nagaosa, and Y. Tokura, Real-space observation of a two-dimensional skyrmion crystal, *Nature (London)* **465**, 901 (2010).
- [10] A. N. Bogdanov and D. A. Yablonskii, Thermodynamically stable “vortices” in magnetically ordered crystals. The mixed state of magnets, *Sov. Phys. JETP* **68**, 101 (1989).
- [11] A. K. Nayak, V. Kumar, T. Ma, P. Werner, E. Pippel, R. Sahoo, F. Damay, U. K. Röbber, C. Felser, and S. S. P. Parkin, Magnetic antiskyrmions above room temperature in tetragonal Heusler materials, *Nature (London)* **548**, 561 (2017).
- [12] W. Koshibae and N. Nagaosa, Theory of antiskyrmions in magnets, *Nat. Commun.* **7**, 10542 (2016).
- [13] N. Kanazawa, M. Kubota, A. Tsukazaki, Y. Kozuka, K. S. Takahashi, M. Kawasaki, M. Ichikawa, F. Kagawa, and Y. Tokura, Discretized topological Hall effect emerging from skyrmions in constricted geometry, *Phys. Rev. B* **91**, 041122(R) (2015).
- [14] H. Barkhausen, Zwei mit Hilfe der neuen verstärker entdeckte erscheinungen, *Z. Phys.* **20**, 401 (1919).
- [15] D. Shimizu, T. Nagase, Y.-G. So, M. Kuwahara, N. Ikarashi, and M. Nagao, Nanoscale characteristics of a room-temperature coexisting phase of magnetic skyrmions and antiskyrmions for skyrmion-antiskyrmion-based spintronic applications, *ACS Appl. Nano Mater.* **5**, 13519 (2022).
- [16] F. S. Yasin, L. Peng, R. Takagi, N. Kanazawa, S. Seki, Y. Tokura, and X. Yu, Bloch lines constituting antiskyrmions captured via differential phase contrast, *Adv. Mater.* **32**, 2004206 (2020).
- [17] K. Karube, L. Peng, J. Masell, X. Yu, F. Kagawa, Y. Tokura, and Y. Taguchi, Room-temperature antiskyrmions and sawtooth

- surface textures in a non-centrosymmetric magnet with S_4 symmetry, *Nat. Mater.* **20**, 335 (2021).
- [18] L. Peng, K. V. Iakoubovskii, K. Karube, Y. Taguchi, Y. Tokura, and X. Yu, Formation and control of zero-field antiskyrmions in confining geometries, *Adv. Sci.* **9**, 2202950 (2022).
- [19] Z. He, D. Song, W. Wang, N. Wang, B. Ge, S. Wang, M. Tian, and H. Du, Visualizing emergent magnetic flux of antiskyrmions in $Mn_{1.4}PtSn$ magnet, *Adv. Funct. Mater.* **32**, 2112661 (2022).
- [20] A. O. Leonov, T. L. Monchesky, N. Romming, A. Kubetzka, A. N. Bogdanov, and R. Wiesendanger, The properties of isolated chiral skyrmions in thin magnetic films, *New J. Phys.* **18**, 065003 (2016).
- [21] J. Jena, B. Göbel, V. Kumar, I. Mertig, C. Felser, and S. Parkin, Evolution and competition between chiral spin textures in nanostripes with D_{2d} symmetry, *Sci. Adv.* **6**, eabc0723 (2020).
- [22] J. Jena, B. Göbel, T. Ma, V. Kumar, R. Saha, I. Mertig, C. Felser, and S. S. P. Parkin, Elliptical Bloch skyrmion chiral twins in an antiskyrmion system, *Nat. Commun.* **11**, 1115 (2020).
- [23] M. Heigl, S. Koraltan, M. Vaňatka, R. Kraft, C. Abert, C. Vogler, A. Semisalova, P. Che, A. Ullrich, T. Schmidt *et al.*, Dipolar-stabilized first and second-order antiskyrmions in ferrimagnetic multilayers, *Nat. Commun.* **12**, 2611 (2021).
- [24] L. Camosi, N. Rougemaille, O. Fruchart, J. Vogel, and S. Rohart, Micromagnetics of antiskyrmions in ultrathin films, *Phys. Rev. B* **97**, 134404 (2018).
- [25] S. Huang, C. Zhou, G. Chen, H. Shen, A. K. Schmid, K. Liu, and Y. Wu, Stabilization and current-induced motion of antiskyrmion in the presence of anisotropic Dzyaloshinskii-Moriya interaction, *Phys. Rev. B* **96**, 144412 (2017).
- [26] M. Hoffmann, B. Zimmermann, G. P. Müller, D. Schürhoff, N. S. Kiselev, C. Melcher, and S. Blügel, Antiskyrmions stabilized at interfaces by anisotropic Dzyaloshinskii-Moriya interactions, *Nat. Commun.* **8**, 308 (2017).
- [27] K. Karube, L. Peng, J. Masell, M. Hemmida, H. A. Krug von Nidda, I. Kézsmárki, X. Yu, Y. Tokura, and Y. Taguchi, Doping control of magnetic anisotropy for stable antiskyrmion formation in schreibersite $(Fe, Ni)_3P$ with S_4 symmetry, *Adv. Mater.* **34**, 2108770 (2022).
- [28] See Supplemental Material at <http://link.aps.org/supplemental/10.1103/PhysRevB.108.104403> for details.
- [29] S. Sen, C. Singh, P. K. Mukharjee, R. Nath, and A. K. Nayak, Observation of the topological Hall effect and signature of room-temperature antiskyrmions in Mn-Ni-Ga D_{2d} Heusler magnets, *Phys. Rev. B* **99**, 134404 (2019).
- [30] S. Sugimoto, Y. Takahashi, and S. Kasai, Transition of topological Hall effect for tetragonal Heusler Mn_2PtSn thin film, *Appl. Phys. Express* **14**, 103003 (2021).
- [31] S. Sen, K. Somesh, R. Nath, and A. K. Nayak, Manipulation of Antiskyrmion Phase in $Mn_{2+x}Ni_{1-x}Ga$ Tetragonal Heusler System, *Phys. Rev. Appl.* **17**, 044040 (2022).
- [32] M. Winter, F. J. T. Goncalves, I. Soldatov, Y. He, B. E. Z. Céspedes, P. Milde, K. Lenz, S. Hamann, M. Uhlarz, P. Vir *et al.*, Antiskyrmions and their electrical footprint in crystalline mesoscale structures of $Mn_{1.4}PtSn$, *Commun. Mater.* **3**, 102 (2022).
- [33] P. Vir, J. Gayles, A. S. Sukhanov, N. Kumar, F. Damay, Y. Sun, J. Kübler, C. Shekhar, and C. Felser, Anisotropic topological Hall effect with real and momentum space Berry curvature in the antiskyrmion-hosting Heusler compound $Mn_{1.4}PtSn$, *Phys. Rev. B* **99**, 140406(R) (2019).
- [34] V. Kumar, N. Kumar, M. Reehuis, J. Gayles, A. S. Sukhanov, A. Hoser, F. Damay, C. Shekhar, P. Adler, and C. Felser, Detection of antiskyrmions by topological Hall effect in Heusler compounds, *Phys. Rev. B* **101**, 014424 (2020).
- [35] M. Hehn, S. Padovani, K. Ounadjela, and J. P. Bucher, Nanoscale magnetic domain structures in epitaxial cobalt films, *Phys. Rev. B* **54**, 3428 (1996).
- [36] J. A. Cape and G. W. Lehman, Magnetic domain structures in thin uniaxial plates with perpendicular easy axis, *J. Appl. Phys.* **42**, 5732 (1971).
- [37] C. Kooy and U. Enz, Experimental and theoretical study of the domain configuration in thin layers of $BaFe_{12}O_{19}$, *Philips Res. Rep.* **15**, 7 (1960).
- [38] B. E. Z. Céspedes, P. Vir, P. Milde, C. Felser, and L. M. Eng, Critical sample aspect ratio and magnetic field dependence for antiskyrmion formation in $Mn_{1.4}PtSn$ single crystals, *Phys. Rev. B* **103**, 184411 (2021).
- [39] Y. He, T. Helm, I. Soldatov, S. Schneider, D. Pohl, A. K. Srivastava, A. K. Sharma, J. Kroder, W. Schnelle, R. Schaefer *et al.*, Nanoscale magnetic bubbles in $Nd_2Fe_{14}B$ at room temperature, *Phys. Rev. B* **105**, 064426 (2022).
- [40] T. Ma, A. K. Sharma, R. Saha, A. K. Srivastava, P. Werner, P. Vir, V. Kumar, C. Felser, and S. S. P. Parkin, Tunable magnetic antiskyrmion size and helical period from nanometers to micrometers in a D_{2d} Heusler compound, *Adv. Mater.* **32**, 2002043 (2020).
- [41] Z. Liu, Topological spin textures of antiskyrmionic crystals in two-dimensional magnetic monolayers, *J. Magn. Magn. Mater.* **539**, 168369 (2021).
- [42] G. Zheng, M. Pardavi-Horvath, X. Huang, B. Keszei, and J. Vandlik, Experimental determination of an effective demagnetization factor for nonellipsoidal geometries, *J. Appl. Phys.* **79**, 5742 (1996).
- [43] A. Vansteenkiste, J. Leliaert, M. Dvornik, M. Helsen, F. Garcia-Sanchez, and B. Van Waeyenberge, The design and verification of MuMax³, *AIP Adv.* **4**, 107133 (2014).
- [44] S. Blundell, *Magnetism in Condensed Matter (Oxford Master Series in Physics)* (Oxford University Press, New York, 2001).